Supplemental Figures for **"Deposition of Metal-Organic Frameworks Within a Porous Protein Crystal Superstructure"**

Jacob B. DeRoo, Rojina Shrestha†, Alec Jones, Deepa Rajendran, Jon Thai, Rob Tuttle, and Christopher D. Snow and Melissa M. Reynolds

**Supplemental Figure 1**

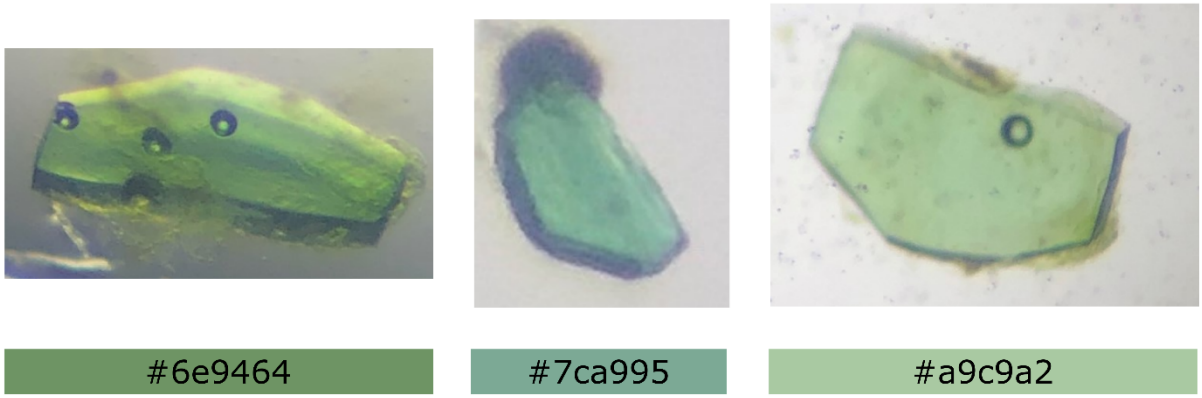


Some CuBTC@CJ crystal photos taken to highlight the color change after growth. These crystals were not taken with a scale bar attached, and subsequently are only used to further illustrate the color change that is observed after interpore and surface CuBTC growth. We can specify that the crystals comfortably fit in the 100 – 150 µm Hampton Research Mounted CryoLoops.

**Supplemental Figure 2**

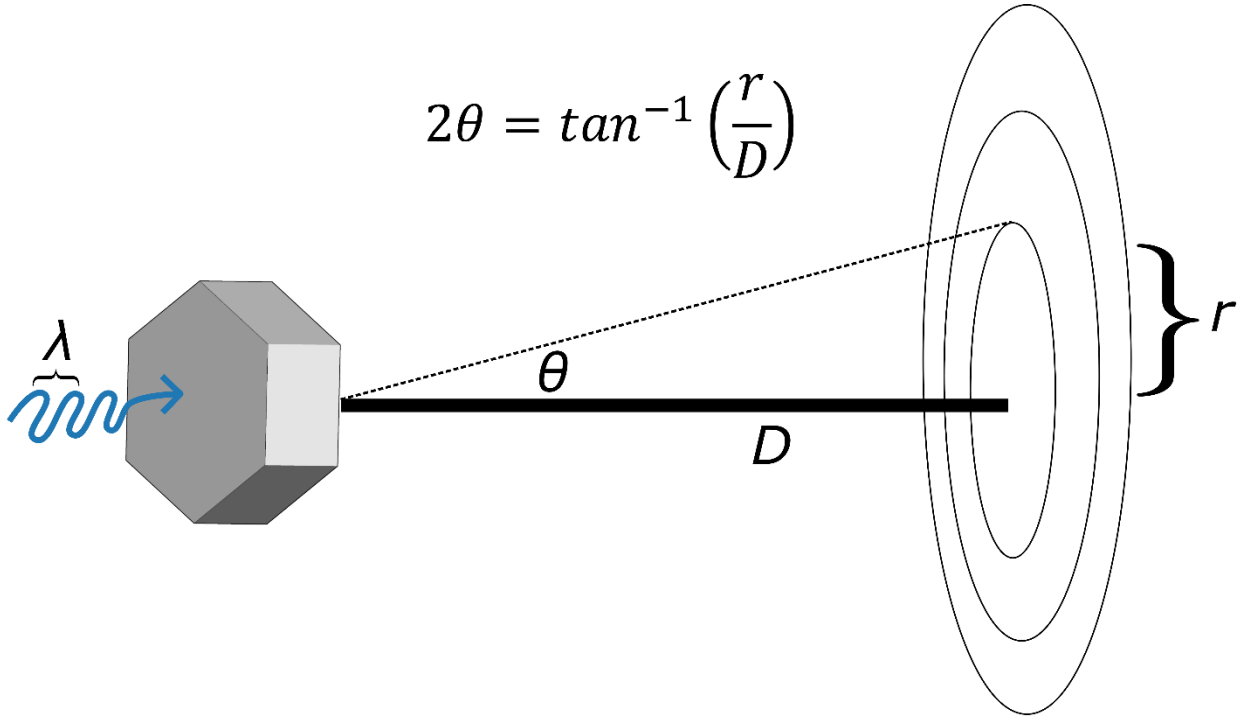


**A physical representation of Debye-Scherrer ring generation in a scXRD experiment.** An X-ray beam strikes the face of a MOF@CJ crystal and is refracted at a certain angle, depending on the orientation of the MOF nanocrystal lattice it strikes. These individual refractions combine to form Debye-Scherrer rings on the detector (x, y, intensity). To create a pXRD plot, we begin at the center of the image, then average all of the pixel intensities at every radial step outwards to create a plot of average intensity vs radius. Radius can then be converted into $2\theta$ to compare the computed pXRD to the expected one. For example scripts, see https://github.com/jbderoo/MOF_in_CJ

**Supplemental Figure 3**

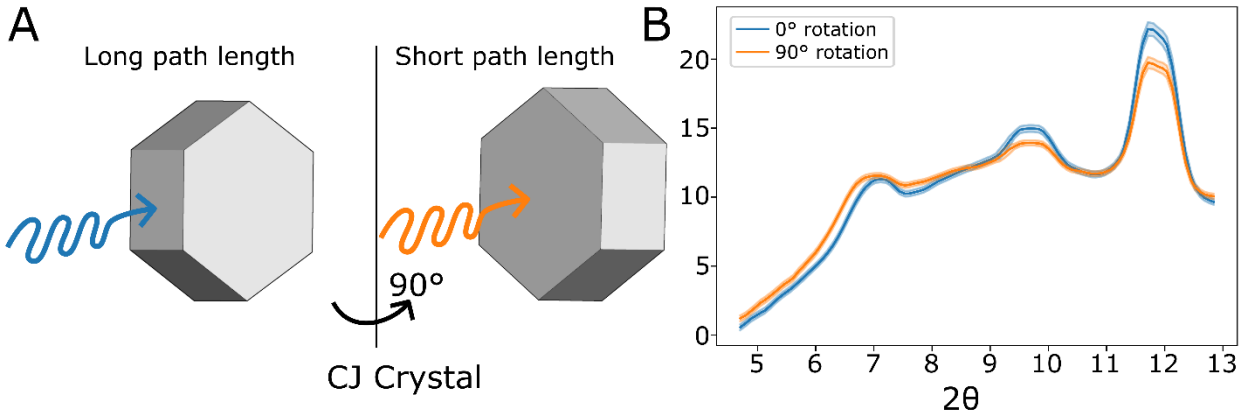


**A)** A CuBTC@CJ crystal was shot at two different orientations. When the X-ray beam was perpendicular to the major nanopore axis (blue) the path length through the crystal interior was longer, when the X-ray beam was parallel to the major nanopore axis (orange), the path length was shorter. **B)** The pXRD plots (+/- 1 standard deviation in intensity along the azimuthal ring, highlighted) of both orientations reveal a clear anisotropy. While there are other possible explanations, the higher diffraction intensity for longer path length is consistent with deposition of CuBTC nanocrystals throughout the CJ crystal interior.

**Supplemental Figure 4**

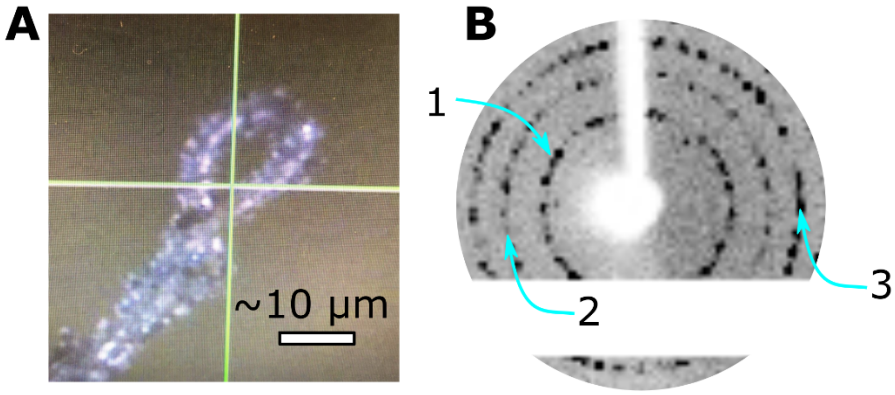


**A)** A picture of a ~10 µm Hampton Research crystallography loop with CuBTC powder pressed into it. **B)** scXRD (taken on the homelab Rigaku) of CuBTC crystals pressed into a fiber loop, then shot on the single crystal diffractometer. This experiment illustrates how the beam passing through individual crystals creates individual Braggs spots. Here, shooting through a moderate number of microcrystals results in distinguishable Bragg spots that are found at the same angle that is populated by Debye-Scherrer rings in a pXRD sample.

**Supplemental Figure 5**

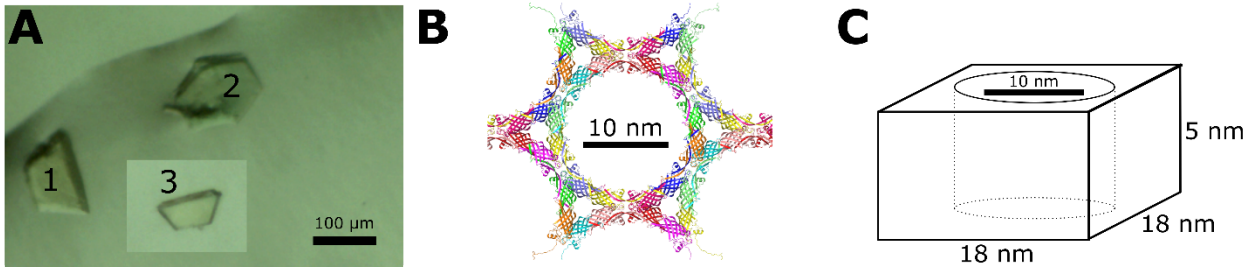


**D**

| Section 1: Total Crystal Volume | | |
|---|---|---|
| Crystal | Shape | Measurement Order |
| 1 | Trapezoidal prism | base, base, width, height |
| 2 | Hexagonal prism | diameter, height |
| 3 | Trapezoidal prism | base, base, width, height |
| Measurement 1 (µm) | | Measurement 2 (µm) |
| 138 | | 74 |
| 66 | | N/A |
| 100 | | 55 |
| Measurement 3 (µm) | | Measurement 4 (µm) |
| 76 | | 17 |
| N/A | | 17 |
| 42 | | 10 |
| Volume (µm$^3$) | | Total volume (µm$^3$) |
| 136952 | | 361894 |
| 192392 | | |
| 32550 | | |

| Section 2: CJ Nanostructure | |
|---|---|
| Diameter of pore (nm) | 13 |
| Depth of pore (nm) | 5 |
| volume of pore (nm$^3$) | 663.7 |
| Total volume (nm$^3$, Section 1) | $3.62 \times 10^{14}$ |
| length of CJ unit cell (nm) | 18 |
| width of CJ unit cell (nm) | 18 |
| volume of CJ unit cell (nm$^3$) | 1403 |
| Number of unit cells (N pores) | $2.58 \times 10^{11}$ |

| Section 3: Copper Quantity via ICP-AES | |
|---|---|
| Cu (µg/L) in water leached from CJ | 0.86 |
| Cu (µg/L) in water (neg control) | 0.03 |
| Cu (µg/L) in water leached due to CJ | 0.83 |
| sample water (mL) sent for analysis | 50 |
| sample water (L) sent for analysis | 0.05 |
| Cu (µg) present in sample | 0.0415 |
| Cu (g) present in sample | $4.15 \times 10^{-8}$ |
| Molecular weight (g/mol) Cu | 63.546 |
| Cu (mol) present in sample | $6.53 \times 10^{-10}$ |
| Cu (atoms) present in sample | $3.93 \times 10^{14}$ |
| Cu (atoms) in a single pore (experimental) | 1524 |

| Section 4: CuBTC packing fraction in CJ | |
|---|---|
| Cu (atoms) in a single pore (theoretical) | 2059 |
| Cu (atoms) in a single pore (experimental) | 1524 |
| Packing fraction CuBTC in CJ (%) | 74 |

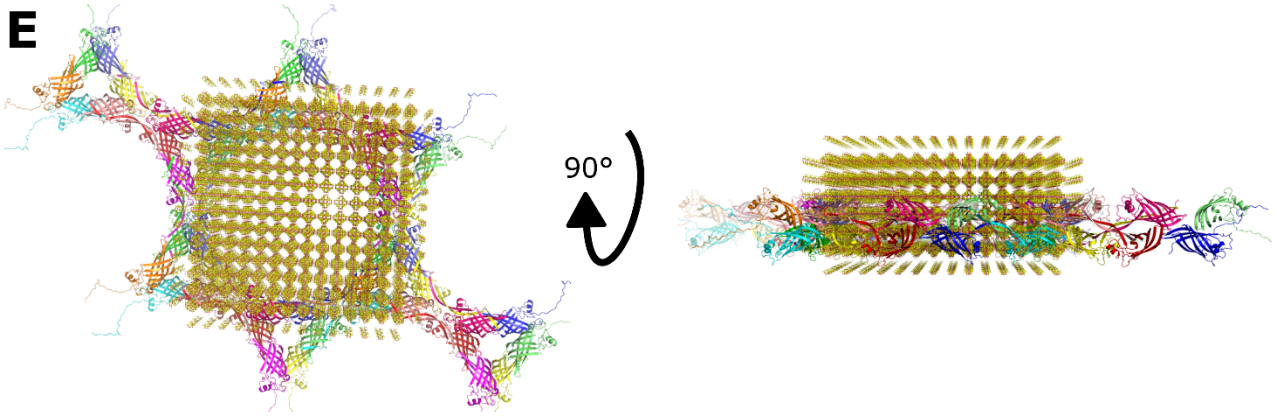

**F**

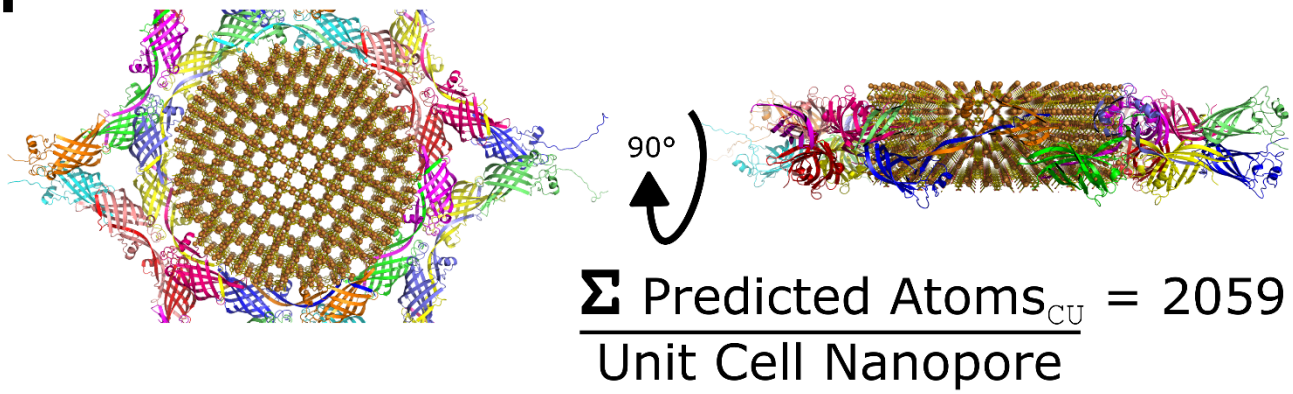


Analysis of the amount of CuBTC that was adsorbed into the CJ protein crystals. **A)** A composite image highlighting the crystals that were used to CuBTC grown inside, then subsequently leached out. Note: crystal 3 had drifted very far from crystals 1 & 2, and the image was composited for ease of visualization. Crystals images were taken prior to CuBTC growth and leaching. **B)** The crystal structure of the CJ protein, PDB code 5W17. **C)** The geometry of the CJ crystal nanostructure, highlighting the 13 nm diameter pore and the 18 nm unit cell. The total volume of the CJ unit cell is approximately 1403 $nm^3$, but not all of this volume is available for a guest MOF – only the interior cylindrical pore is accessible, with a volume of 663.7 $nm^3$. **D)** A four-section, step-by-step explanation of the calculation of the 74% packing fraction. First, measurements of the crystals in **A)** were taken via ImageJ, enabling a calculation of protein volume (**D, Section 1**). The total pore volume and unit cell volume was calculated, then finally a total number of unit cells (**D, Section 2**). The copper concentration was determined experimentally by Huffman Hazen in Golden, CO via ICP-AES (**D, Section 3**). The theoretical amount of CuBTC that could fit inside the CJ pore was determined by creating a large, structured grid of CuBTC and overlaying this on the CJ structure (**E**). The MOF was then limited to exist only just beyond the major axial nanopore (13.5 nm diameter) the pore wall, and then a final clash detection step was used to create a perfect fit between the MOF and the solvent accessible surface of the CJ nanopore (**F**). This is analogous to taking a ring mold (CJ nanostructure) and using it to cut perfect, evenly sized cookies from a sheet of cookie dough (large CuBTC grid). The total number of copper atoms (per unit-cell nanopore) were finally estimated as

2060 atoms per CJ pore. With a theoretical maximum number of Cu atoms and an experimental number of Cu atoms determined via leaching, a packing fraction of 74% is calculated (**D, Section 3**). Scripts for calculating the theoretical maximum number of Cu atoms in the pore can be found in our github at https://github.com/jbderoo/MOF_in_CJ .

**Supplemental Figure 6**

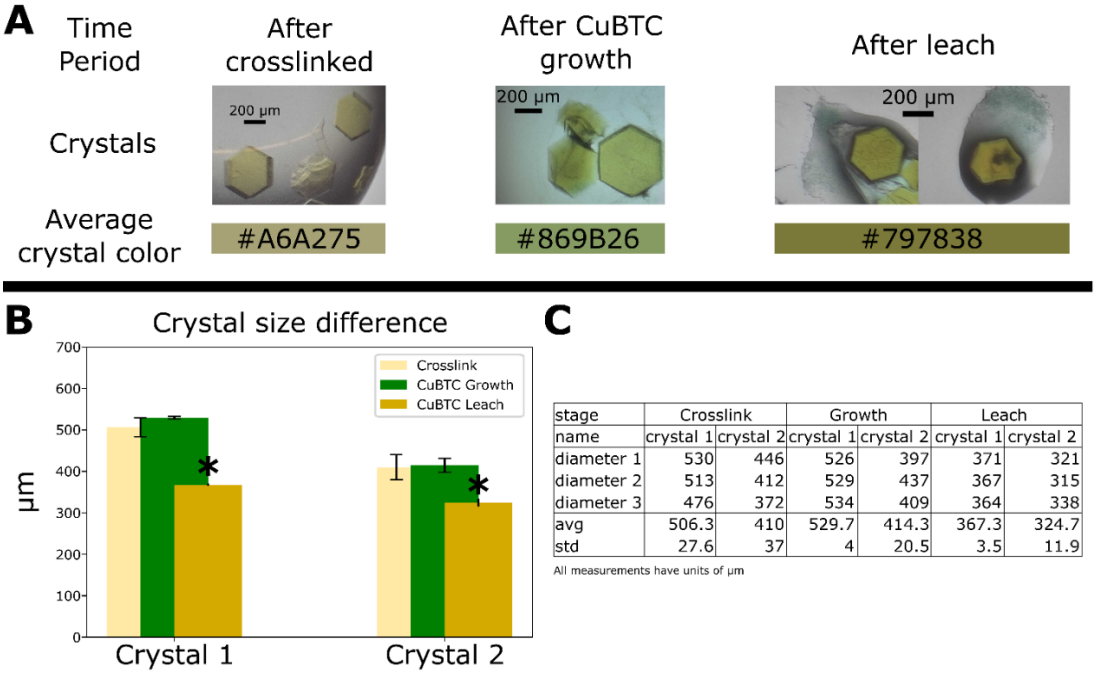


| stage | Crosslink | | Growth | | Leach | |
|---|---|---|---|---|---|---|
| name | crystal 1 | crystal 2 | crystal 1 | crystal 2 | crystal 1 | crystal 2 |
| diameter 1 | 530 | 446 | 526 | 397 | 371 | 321 |
| diameter 2 | 513 | 412 | 529 | 437 | 367 | 315 |
| diameter 3 | 476 | 372 | 534 | 409 | 364 | 338 |
| avg | 506.3 | 410 | 529.7 | 414.3 | 367.3 | 324.7 |
| std | 27.6 | 37 | 4 | 20.5 | 3.5 | 11.9 |

All measurements have units of µm

Analysis of the change in size and color of CJ crystals before and after CuBTC had been grown inside them. **A)** 2 ideal crystals are shown after crosslinking but before CuBTC growth (left), after CuBTC growth but before CuBTC leaching (middle) and after CuBTC leaching into water (right). CuBTC was allowed to grow for 24 hours and leach out of the CJ crystals for 24 hours. Additionally, the average color of the crystals is provided both as a color and its corresponding hex color code. Interestingly, partially formed CuBTC or CuBTC components were visible outside the CJ crystal after leaching. **B)** Crystals were analyzed for size change with ImageJ, and each of the 3 treatments are plotted for both crystals' diameters. There was a statistically significant shrinkage in the crystals after leaching, but this is likely due to the drops being allowed to nearly dry out rather than due to MOF dissolution. Shrinking during desiccation also explains the phenomenon of the crystal becoming a darker yellow; the crystal is shrinking, but the number of blue-light-adsorbing glyoxal end products remains the same, thus increasing the spatial density of the yellow color. **C)** The raw data (in µm) used to generate the plots in **B)**.

**Supplemental Figure 7**

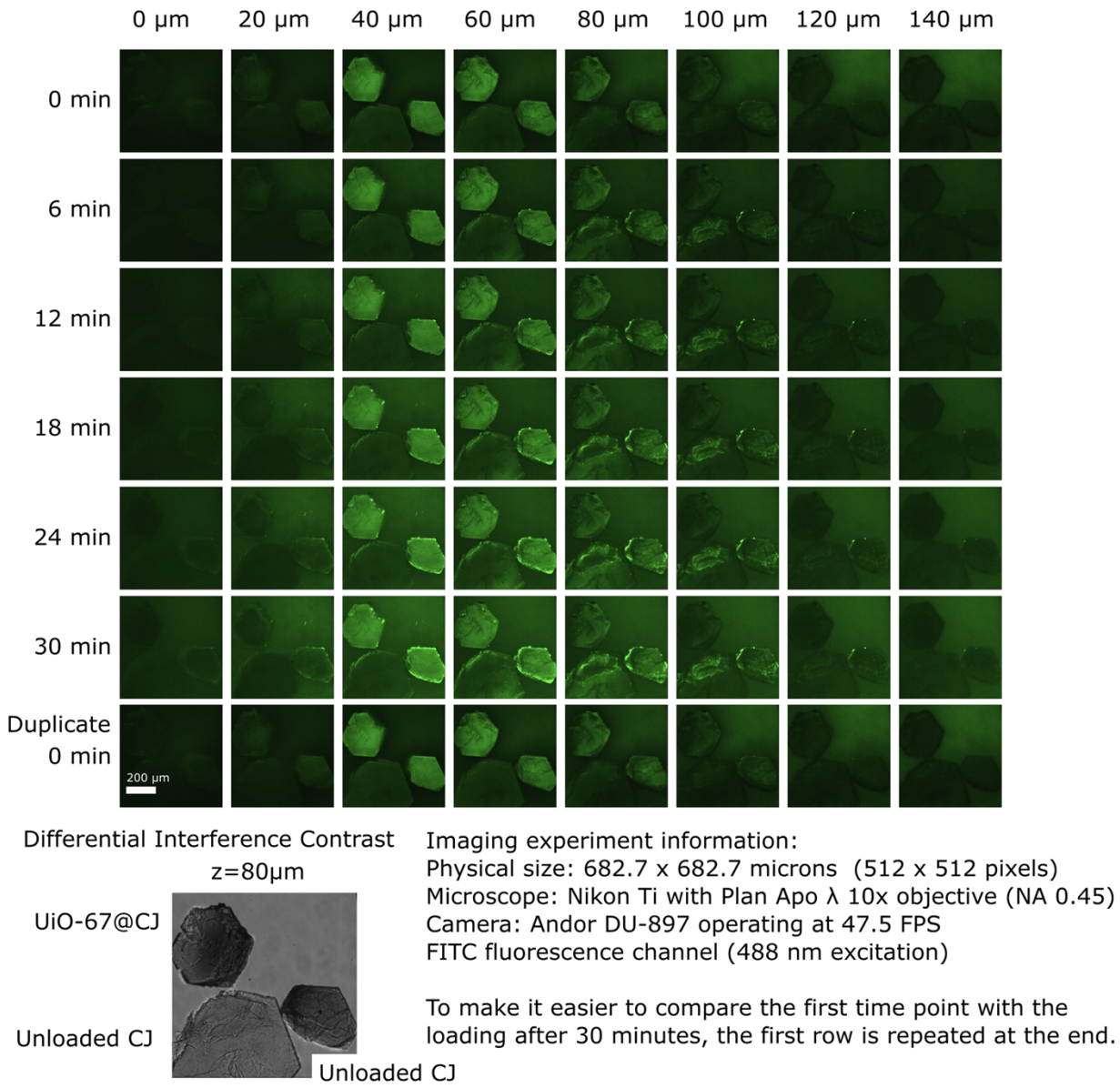


Confocal microscopy images of the CJ crystals under various loading and growth conditions. The top left crystal is the UiO-67@CJ crystal. The bottom left is an unloaded CJ crystal. The bottom right is an additional unloaded CJ crystal that floated into frame and stayed during the experiment. The images horizontally right are moving down the depth of the crystal in the Z-stack; moving vertically down are increasing as time goes on. The 0-time row of images is duplicated for convenience.

**Supplemental Figure 8**

To further bolster the evidence that the MOF deposition chemistry effects changes throughout the CJ crystal interior, rather than just the surface, we undertook confocal microscopy on two large crystals. Specifically, we performed z-depth resolved imaging of two crystals before (DepositionInitial.mp4) and 1 hour after exposure to CuBTC deposition chemistry (DepositionFinal.mp4). We also performed time-resolved imaging of internal z-planes for the two crystals for 30 minutes after triggering putative MOF deposition (DepositionTimeLapse.mp4). All videos are hosted on the Google Drive link (https://drive.google.com/drive/folders/1GaK_t8EFntWVmi9jq2cfTvgqhMo6voNe?usp=drive_link).

CJ crystals were grown and cross-linked as described in the methods section. After cross-linking and quenching, the crystals were then imaged in deionized water (DepositionInitial.mp4), then transferred to 30 µL of CuBTC MOF precursor solution (245 g/L $Cu(NO_3)_2$, 116 g/L BTC in DMSO, as described in methods). After approximately 5 minutes, MOF growth was initiated via addition of 30 µL of 1.2 M HCl, and imaged every 30 seconds for approximately 50 minutes (DepositionTimeLapse.mp4). The crystals were then looped back into deionized water, and imaged a final time (DepositionFinal.mp4). Images were obtained as a ratio of green fluorescence of the guest CuBTC MOF (488/530), to blue autofluorescence associated with the CJ crystal (405/460).

As mentioned in Supplemental Figure 9, we had previously noted possible changes in green fluorescence when CJ crystals were subjected to CuBTC deposition. Therefore, to sensitively assess changes within the crystals we used a ratiometric approach: all frames in the provided z-stacks and time-lapse videos are false color depictions of the fluorescence emission ratio: emissions with 488 nm excitation divided by emissions with 405 nm excitation.

The scale is: red = 2.0X, green = 1.0X, purple = 0X. T.

For readers who prefer still images over the videos here are selected frames.

Evenly spaced frames from the time lapse: $\frac{I_{488ex}}{I_{405ex}}$. In this series, both crystals are hexagonal prisms with their 6-fold axis perpendicular to z, resulting in rectangular cross-sections:

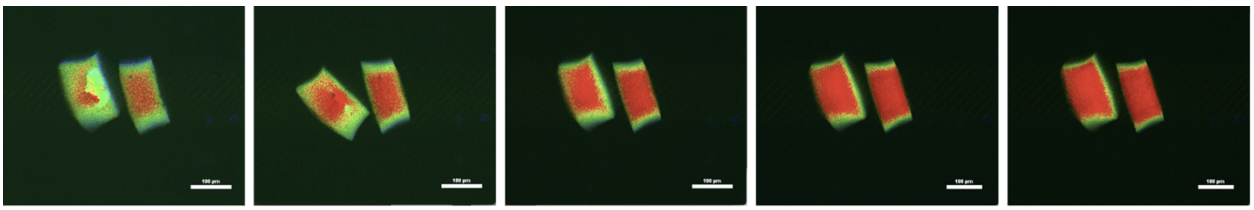

Selected z-layers for the crystals prior to addition of 30 µL of 1.2 M HCl: $\frac{I_{488ex}}{I_{405ex}}$. In this case, one of the two crystals has turned so that its 6-fold axis is aligned with z.

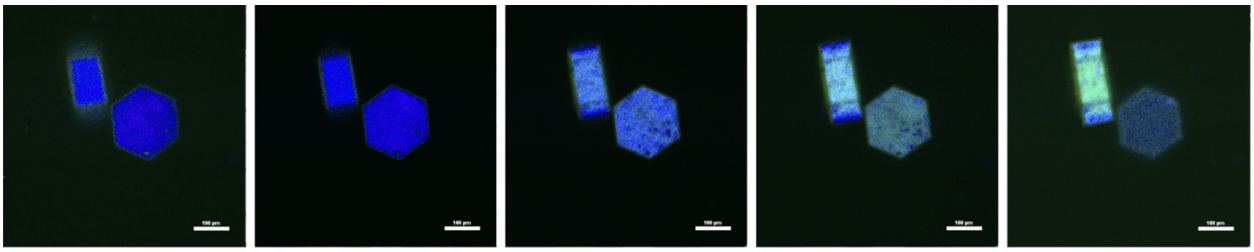

Selected z-layers for the crystals X minutes after addition of 30 µL of 1.2 M HCl: $\frac{I_{488ex}}{I_{405ex}}$. In this series, both crystals have turned so that their 6-fold axes are aligned with z.

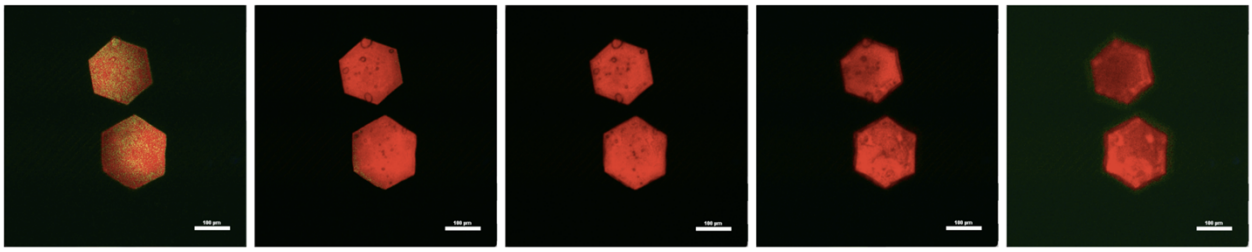

As seen in both the before and after images, and the time lapse crystal cross-section, we observed a significant increase in the green emission relative to the blue emission $\frac{I_{488ex}}{I_{405ex}}$, after subjecting the crystals to the conditions intended to trigger CuBTC growth.

**Supplemental Figure 9**

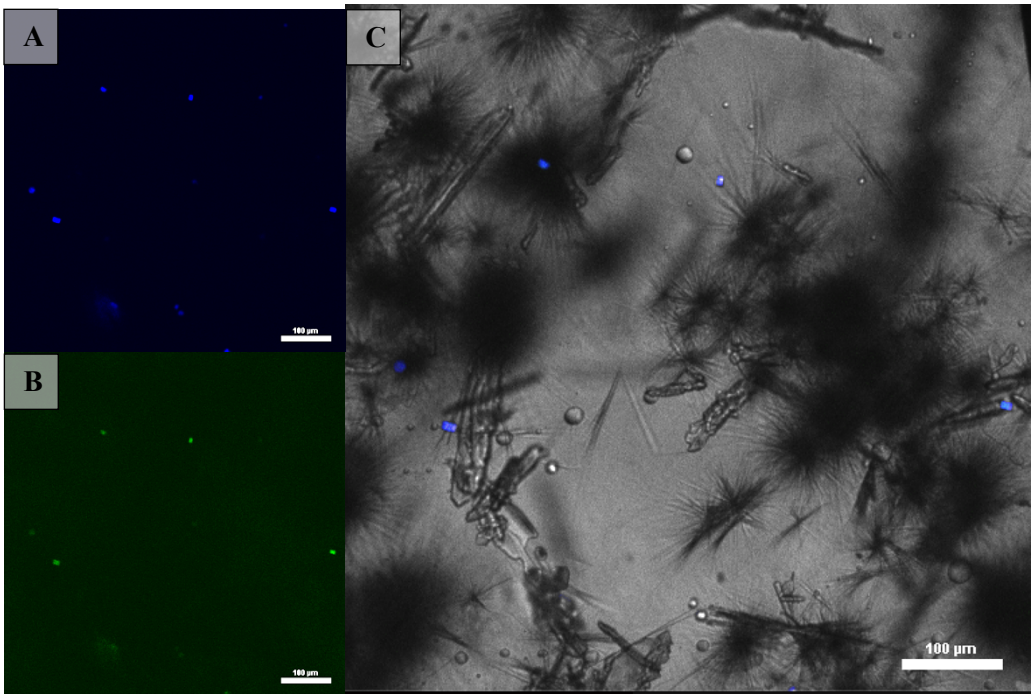


Unloaded CJ crystals or CuBTC@CJ crystals, (A) imaged using Pacific Blue settings ($\lambda_{ex}$ = 405 nm, $\lambda_{em}$ = 452 nm) or (B) FITC settings ($\lambda_{ex}$ = 488 nm, $\lambda_{em}$ = 530 nm). One potentially interesting observation was an increase in green light emission observed for putative CuBTC@CJ microcrystals, relative to comparable empty CJ microcrystals (not shown). (C) Both blue and green are merged with the differential interference contrast (DIC) channel, revealing that the CJ microcrystals are surrounded by diverse CuBTC microcrystal overgrowth. While the DIC channel carries no color, the CuBTC crystals were blue when inspected with white light microscopy (not shown), consistent with Supplemental Figure 1.

**Supplemental Figure 10**

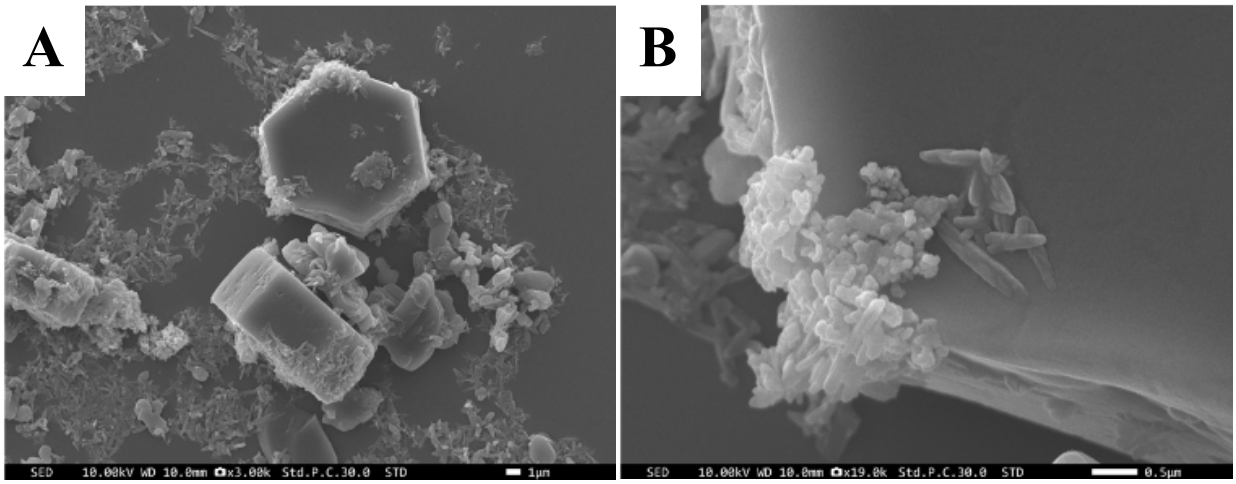


Panels A and B contain two magnifications of SEM data collected for UiO-67 grown in the presence of CJ microcrystals (hexagonal prisms) rather than the much larger CJ crystals used in Figure 4. The new higher magnification in panel B allows the observation of particles that we hypothesize are UiO-67 nanocrystals, despite the lack of the regular octahedron UiO-67 crystal habit.

**Footnotes**

† Deceased